Check for updates

A highly efficient triboelectric negative air ion generator

Hengyu Guo [1,2,3,6], Jie Chen[2,3,6], Longfei Wang [1,2,6], Aurelia Chi Wang[2], Yafeng Li [2], Chunhua An[2], Jr-Hau He [4], Chenguo Hu [3], Vincent K. S. Hsiao [2,5] ✉ and Zhong Lin Wang [1,2] ✉

Negative air ions (NAIs) have been widely harnessed in recent technologies for air pollutant removal and their beneficial effects on human health, including allergy relief and neurotransmitter modulation. Herein, we report a corona-type, mechanically stimulated triboelectric NAI generator. Using the high output voltage from a triboelectric nanogenerator, air molecules can be locally ionized from carbon fibre electrodes through various movements, with the electron–ion transformation efficiency reaching up to 97%. Using a palm-sized device, 1×10^{13} NAIs (theoretically 1×10^5 ions cm^{-3} in 100 m^3 space) are produced in one sliding motion, and particulate matter (PM 2.5) can be rapidly reduced from 999 to 0 µg m^{-3} in 80 s (in a 5,086 cm^3 glass chamber) under an operation frequency of 0.25 Hz. This triboelectric NAI generator is simple, safe and effective, providing an appealing alternative, sustainable avenue to improving health and contributing to a cleaner environment.

N egative air ions (NAIs), known as 'air vitamins', are small ions with an average electric mobility of 1–2 cm^2 V^{-1} s^{-1}. They are widely used for indoor air purification, including the removal of airborne particulate matter, the oxygenolysis of volatile organic compounds and bacteriostasis, and have been proven to be beneficial to both the physiological and psychological health of humans and other animals[1–6]. Aside from NAI production from natural sources, such as forests, waterfalls and rainstorms, NAI generators based on corona discharges, thermionic electron emission, photoexcitation and the Lenard effect have been developed for creating NAIs artificially[7]. Among these mechanisms, corona-type NAI generators based on high electric field-induced air ionization near a needle electrode have been commercialized and are the most commonly employed variant[8–10]. Even so, a voltage-boosting circuit module is used to yield a high voltage for the needle electrode[10], which has a number of shortcomings, such as complicated circuitry, cumbersome size and hazardous properties (for example, they cannot be touched without a protective circuit), largely limiting the diversity in applications of existing corona NAI generators. As alternatives, the reaction between water and pyroelectric crystals to generate NAIs[11] or the release of NAIs from mixed pyroelectric compounds by mechanical pressure[12] have been explored. However, the NAI concentrations generated by these methods are low, and the sources of mechanical stimulation used require variety and applicability in real-life situations. Thus, at this stage, there lacks an optimized, facile technology for the artificial enrichment of NAIs, which is highly desirable for their sustainable commercialization.

Recently, based on the coupling of triboelectrification and electrostatic induction, triboelectric nanogenerators (TENGs) that can convert various ambient mechanical motions into electricity have been developed with the advantages of being lightweight, flexible, easily fabricated and low-cost, as well as having a wide selection of possible materials[13–23]. Compared with traditional electromagnetic generators, TENGs perform with higher efficiency at low frequency (<5 Hz)[24], and their intrinsic features of high voltage (~kV) and low current (~µA) also render TENGs as novel high-voltage power (HV) sources with unprecedented portability and safety. TENGs can easily produce high voltages of over 10 kV without complicated converter circuits, which greatly simplifies the system and reduces cost[14]. TENGs have been proven an efficient HV supply for driving nanoelectrospray ionization[25], electrospinning[26], electron field emission[27] and microplasma production[28]. With these capabilities, TENG-based HV sources provide a simple and feasible solution for artificial NAI generation.

Herein, we report the first prototype of a motion-stimulated triboelectric NAI generator driven by a TENG. Both a free-standing (FS-) and contact-separation (CS-) TENG, which can convert mechanical movement into electricity, have been applied as HV sources. The production of a voltage of over 2,000 V from a carbon fibre electrode is easily achieved and the electron–ion transformation efficiency reaches up to 97 and 70% for the FS-TENG and CS-TENG, respectively. The generated NAIs were characterized using mass spectrometry and the air ionization processes were theoretically analysed in detail by studying the voltage–charge (V–Q) loops of the TENGs. In one operational period, palm-sized FS- and CS-TENG devices produce 2×10^{13} NAIs (theoretically 2×10^5 ions cm^{-3} in a 100 m^3 space) and 1.5×10^{12} NAIs (theoretically 1.5×10^4 ions cm^{-3} in a 100 m^3 space), respectively. We also demonstrate that particulate matter (PM) 2.5 in an enclosed glass chamber (5,086 cm^3) quickly declines from 999 to 0 µg m^{-3} in 80 s under an operational frequency of the TENG devices of 0.25 Hz. The reported triboelectric NAI generator has great potential to contribute to the diversity in economic, facile and safe artificial NAI generation.

Results

Design and characterization of motion-stimulated NAI generator. Corona discharge is a mechanism widely used for developing artificial NAI generators. In this work, using the high output voltage

[1]Beijing Institute of Nanoenergy and Nanosystems, Chinese Academy of Sciences, Beijing, People's Republic of China. [2]School of Materials Science and Engineering, Georgia Institute of Technology, Atlanta, GA, USA. [3]Department of Applied Physics, State Key Laboratory of Power Transmission Equipment and System Security and New Technology, Chongqing University, Chongqing, People's Republic of China. [4]Department of Materials Science and Engineering, City University of Hong Kong, Hong Kong, China. [5]Department of Applied Materials and Optoelectronic Engineering, National Chi Nan University, Nantou, Taiwan. [6]These authors contributed equally: Hengyu Guo, Jie Chen, Longfei Wang. ✉e-mail: kshsiao@ncnu.edu.tw; zhong.wang@mse.gatech.edu
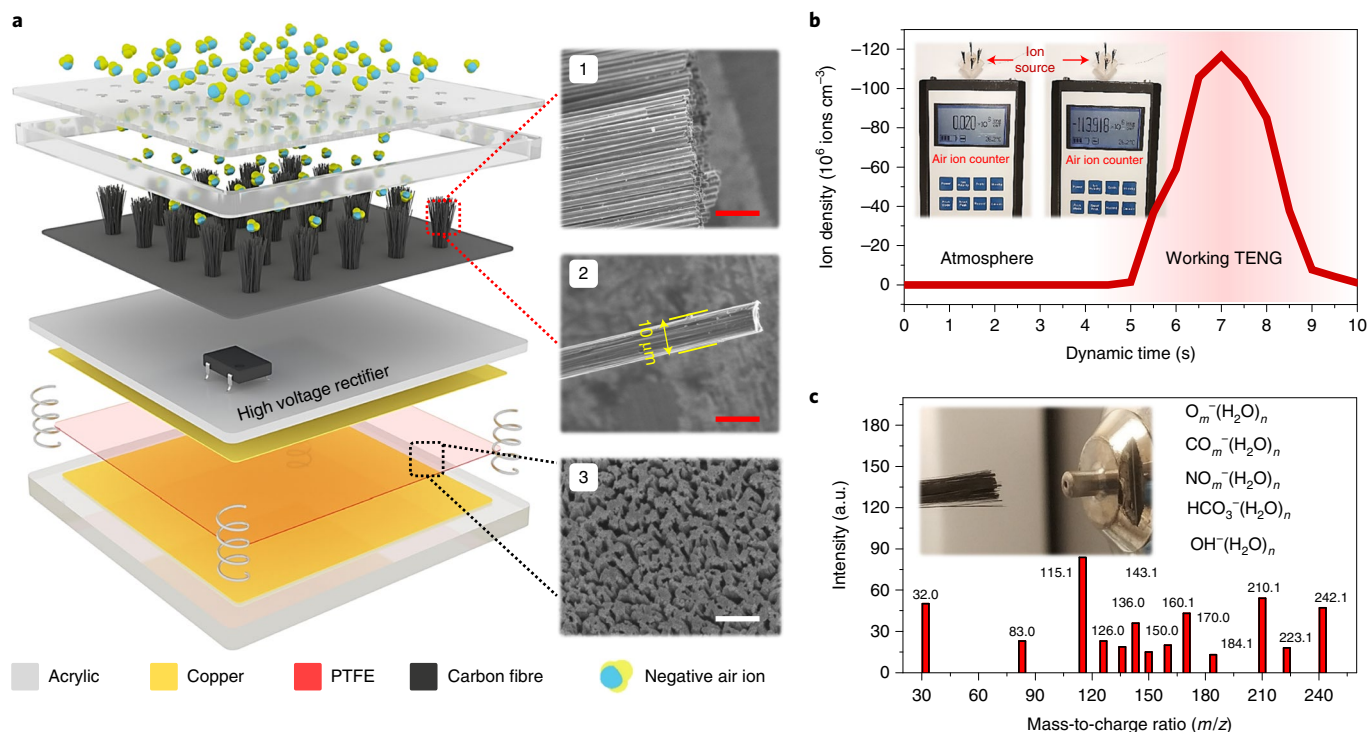
Fig. 1 | Prototype of the MSNG. a, Three-dimensional schematic of the motion-driven air ionizer that consists of a TENG component, high-voltage rectifier module and carbon fibre electrode array layer. Insets 1 (scale bar, 100 μm) and 2 (scale bar, 10 μm) show scanning electron microscopy images of bunched and individual carbon fibres, respectively. Inset 3 shows the surface morphology of the tribo-layer (scale bar, 1 μm). PTFE, polytetrafluoroethylene. **b**, Time-dependent variation of the NAI density, monitored by an ion air counter (inset), when operating the TENG. **c**, Identification of the NAI species generated at the TENG-actuated carbon fibre electrodes using mass spectrometry. The inset shows a photograph of the carbon fibre electrodes and the input channel of mass spectrometry.

of a TENG and carbon fibre electrodes, we developed the prototype of a portable, highly efficient and motion-stimulated NAI generator (MSNG). As the three-dimensional schematic in Fig. 1a illustrates, the MSNG is a simply structured and highly integrated device that mainly consists of a TENG component, a high-voltage rectifier circuit module and carbon fibre array electrodes. Insets 1 and 2 of Fig. 1a show the scanning electron microscopy images of bunched and individual carbon fibre electrodes, respectively. The 10 μm diameter of the electrodes promotes the formation of a localized high electric field for air ionization[29,30]. To produce a higher output voltage, the surface of the TENG tribo-layer was etched to form nanostructures (Fig. 1a, inset 3). In our prototype, a CS-TENG converts vertical mechanical motion (for example, vibrations, treading and tapping) into electricity to drive NAI generation at the tip of the carbon electrodes. The complete system has the potential to work as an NAI source in a running automobile, in an industrial factory setting, on an indoor floor and in many other situations. In addition, by replacing the CS-TENG with an FS-TENG to convert horizontal movement (for example, sliding and rotating), the MSNG can also act as a portable device for continuously producing NAIs by harvesting energy from biomechanical input, wind and water flow (Supplementary Fig. 1). The fabrication process of the MSNG is described in detail in the Methods section and the as-fabricated FS-TENG, CS-TENG, rectifier elements and carbon fibre electrodes are shown in Supplementary Fig. 2. An air ion counter is a commonly used instrument for determining the relative amount of air ions in an environment (with mobility $>1\,cm^2\,V^{-1}\,s^{-1}$)[7,31]. In our experiment, we used a commercially available air ion counter to quantitatively verify the levels of NAIs generated by the MSNG. As shown in Fig. 1b, the NAI density dramatically rises from 0 to

$120\times10^6\,ions\,cm^{-3}$ when the incorporated TENG device is operated, which certifies the effectiveness of our TENG-based NAI generator. Moreover, the generated NAI species were further identified by mass spectrometry[7]. From the spectral section shown in Fig. 1c, O^-, O_2^-, O_3^-, O_4^-, CO_2^-, CO_3^-, CO_4^-, NO_2^-, NO_3^-, OH^- and HCO_3^- combined with $(H_2O)_n$ ions were successfully detected. The complete mass spectrum and the list of detected ions are both presented in Supplementary Fig. 3, and match well the known NAIs reported in the literature[32–35]. All the aforementioned preliminary results are substantial proof of the feasibility of generating NAIs by our MSNG.

Quantification of NAIs and maximal output from TENG. Because the sampling rate of a commercialized air ion counter is too low (two samples per second) to accurately measure the total quantity of produced ions, we designed a testing platform for quantitatively monitoring the NAIs. As schematically shown in Fig. 2a, the carbon fibre electrodes are fixed in a glass chamber open on two sides, an air fan is mounted on one side and a conductive silver textile is used to seal the other side. While operating the TENG device, the air fan drives the generated NAIs forward towards the dense and conductive silver textile, which collects most of the charged ions from the air passing through by a ammeter or Coulomb meter. In this way, the total collected charges can be regarded as the NAI quantity. The complete diagram of the testing platform and the effects of air flow on charge collection are both depicted in Supplementary Fig. 4. Using this testing platform, the average currents generated by the collected ions were recorded when applying various negative d.c. voltages. As plotted in Fig. 2b, a diode-like rectifying curve is observed, and the current (corresponding to collected air ions) dramatically increases when the voltage exceeds −2,000 V, which
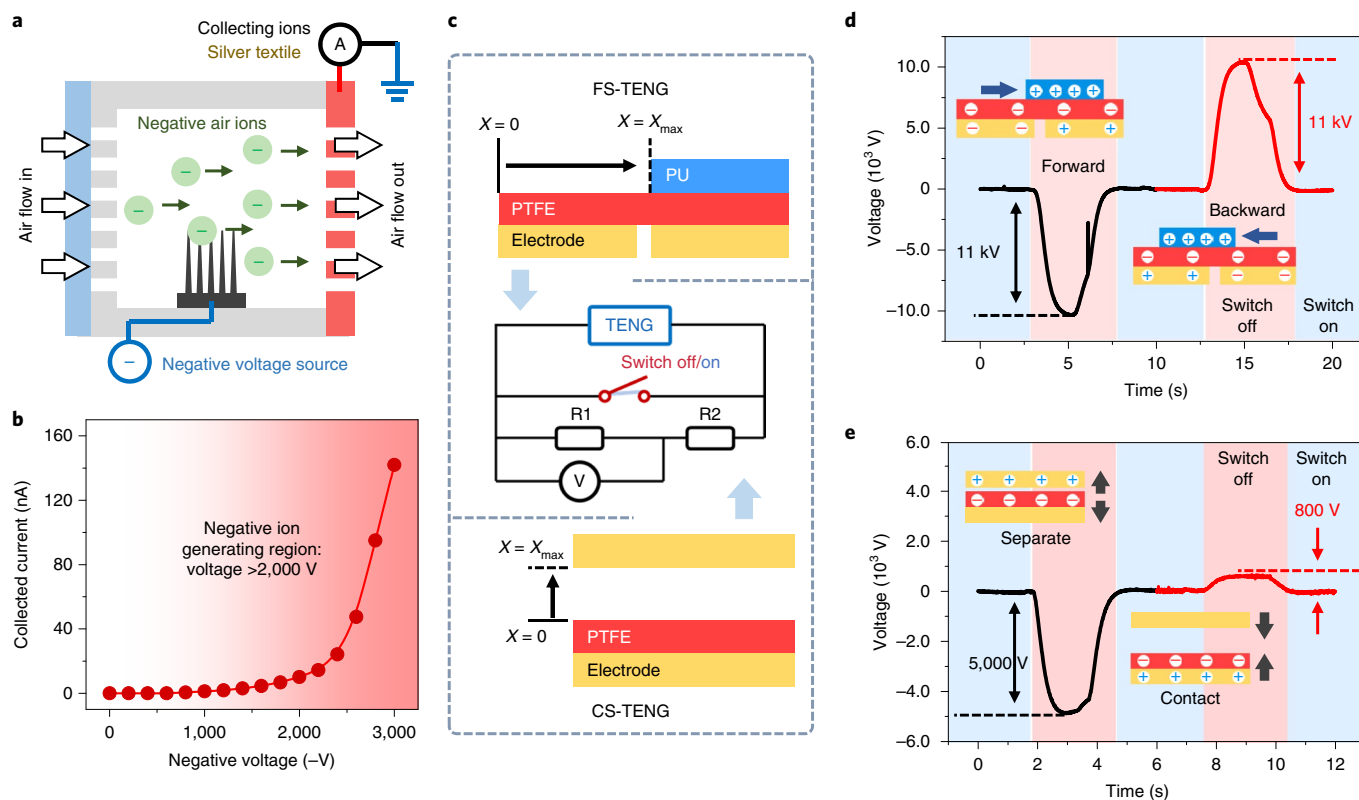
Fig. 2 | Output quantification of TENG for air ionization. a, Schematic of the testing platform used to measure the quantity of NAIs. **b**, The relationship between the average collected ion current and the negative d.c. voltage. **c**, Schematic of the measurement of the maximal open-circuit voltage of the FS- and CS-TENGs. PU, polyurethane. **d**, Output voltage of the FS-TENG during forward and backward steps. **e**, Output voltage of the CS-TENG during separating and contacting steps.

indicates the threshold voltage of effective NAI generation by the carbon fibre electrodes. Additionally, the maximum outputs of the FS- and CS-TENGs were determined to further discuss the MSNG performance. Considering the testing range limitation of the electrometer, a serially connected resistance (~600 Gohm) was used and the voltage was measured over a partial portion (~1 Gohm). To achieve the maximum open-circuit voltage during each TENG operation step, a switch was introduced to reset the potential difference of the two TENG electrodes to the initial state. Figure 2c shows a schematic of the voltage measurement system. Here, we define the initial position of both TENG devices as $X = 0$ and the maximally displaced position as $X = X_{max}$. The testing steps were as follows: (1) switch on (short circuit) at $X = 0$ (sets the potential difference of two electrodes to zero); (2) switch off (open circuit) as the TENG shifts to $X = X_{max}$; (3) switch on (short circuit) when the TENG reaches $X = X_{max}$ (resets the potential difference of two electrodes to zero); (4) switch off (open circuit) as the TENG shifts back to $X = 0$. The steps and charge distribution schemes are illustrated in detail in Supplementary Fig. 5a,c. For the FS-TENG, due to its constant capacitance, the voltage outputs of the forward and backward motion step both reach 11 kV (Fig. 2d). On the other hand, due to the variation in capacitance of the two electrodes in the CS-TENG, the voltage reaches 5,000 V for each separation step and only 800 V for each contact step (Fig. 2e). The open-circuit potential distributions of the FS- and CS-TENGs during the aforementioned testing steps were also simulated using COMSOL Multiphysics software[36], as shown in Supplementary Fig. 5b,d. The results predict that NAIs may be produced in full cycles of the FS-TENG, but only during the separation steps of the CS-TENG. Furthermore, as shown in Supplementary Fig. 6, the short-circuit charge transfer

for each working step reaches ~1.7 μC for the FS-TENG and ~0.35 μC for the CS-TENG. All these results clearly indicate that the TENG-based HV source most definitely satisfies the requirements of air ionization.

Process of TENG-driven NAI generation. The plot of build-up voltage (V) versus total transferred charge (Q) determines the working status of TENG devices, and is usually used to analyse and optimize the TENG working process[37]. Figure 3a,b shows the V–Q curves of the FS- and CS-TENGs, respectively. The purple dotted lines represent the maximum output cycle and can be realized by the aforementioned steps of open-circuit voltage measurement shown in Fig. 2c. It has been verified that TENGs cannot work in excess of their maximum output cycle. Here, we designed switch-controlled processes for maximally using the outputs of the FS- and CS-TENGs under four working statuses depicted schematically in Fig. 3a,b, respectively. At the initial position ($X = 0$), the switch is turned on (short circuit) and the TENG state is recorded in the V–Q plot as (0, 0) (Status I), which means that the voltage and charge transfer between two electrodes are both equal to zero. Then, the FS-TENG is slid forward and the CS-TENG is separated to the maximally displaced position ($X = X_{max}$) under an open-circuit condition (Status II). During this process, the negative potential difference between the carbon fibre electrode and the ground quickly rises to the threshold value (0, V_{ON}), and continuously ionizes air molecules until reaching the next state (Q_{ion}, V_{ON}), as depicted by the red arrows. For simplification, we assumed that no ionization events occur when the voltage is less than the threshold voltage (V_{ON}), while appreciable quantities of ions are formed at and above V_{ON}. Therefore, the generated NAIs can be equated to the total charge
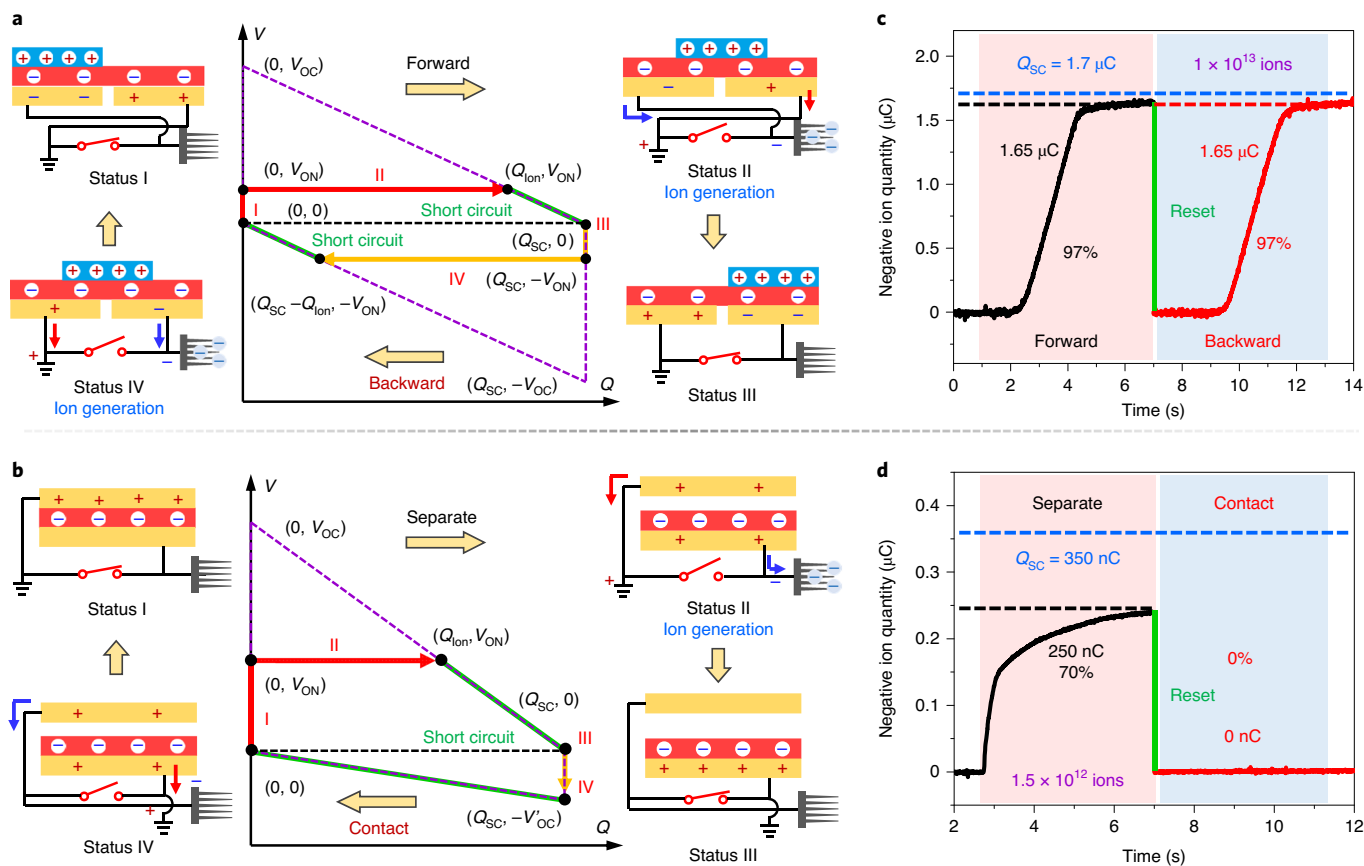
Fig. 3 | Analysis of the working mechanism of the MSNG. a,b, Schematics of the working mechanism and corresponding V–Q curves for NAI generation in one operational period using the FS-TENG (**a**) and CS-TENG (**b**). $-V'_{OC}$ represents the open-circuit voltage during contact motion, which holds a different value to V_{OC}. **c,d**, Time-dependent variation of the generated NAI charge quantity during the forward/backward sliding motion of the FS-TENG (**c**) and the separation/contact motion of the CS-TENG (**d**).

transfer of the TENG in this period. Subsequently, at the maximal position ($X = X_{max}$), the switch is turned on and the residual charges are released to reset both TENG states to (Q_{SC}, 0) (Status III). Following this, the FS-TENG is slid backward and the CS-TENG is depressed to the initial position under an open-circuit condition (Status IV). It is worth noting that, during this backward/contacting process, the electric connection to the TENG electrodes should be reversed to ensure that there is always a negative potential on the carbon electrodes. For the FS-TENG, because the open-circuit voltage reaches the same value in the forward and backward step, the backward process is highly similar to the forward process and the TENG state goes to ($Q_{SC} - Q_{ion}$, $-V_{ON}$) as the yellow arrow indicates in Fig. 3a. Unlike the FS-TENG, for the CS-TENG, there are no NAIs generated on account of the open-circuit voltage (V'_{OC}) during the contacting process being below the threshold value (yellow arrow in Fig. 3b). Finally, at the original position ($X = 0$), the switch is turned on and the state reset to (0, 0) for both the FS- and CS-TENGs for the following operation cycle. The generated NAI quantity in a complete cycle is plotted in Fig. 3c,d. As revealed in Fig. 3c, NAIs with the same charge quantity of ~1.65 μC (equating to 1×10^{13} ions, with the charge quantity of each electron being 1.6×10^{-19} C) are generated by the FS-TENG in both the forward and backward processes. As interpreted on the basis of the short-circuit transferred charge (~1.7 μC), an electron–ion transformation efficiency of 97% is achieved. For the CS-TENG, NAI short-circuit transferred charges of 250 nC (equating to 1.5×10^{12} ions) and 0 nC, with electron–ion transformation efficiencies of 70 and 0%, were measured and calculated

during the separating and contacting processes, respectively, which is also consistent with the theoretical discussion (Fig. 3b). All the aforementioned results and analyses effectively demonstrate the high efficiency and productivity of the MSNGs.

Performance and demonstration of TENG-driven NAI generator. Mechanical switches and reverse circuit connections are inapplicable methods for practical and sustainable NAI generation from natural sources of mechanical energy. In this study, a high-voltage rectifying circuit was integrated into the MSNG to ensure the negative potential of the carbon fibre electrodes during each operational cycle, also driving high-energy electrons for air ionization. Based on the open-circuit voltage features during two basic TENG working cycles, a full-wave rectifier and a single diode element were designed for both the FS- and CS-TENGs, as schematically shown in the insets of Fig. 4a,b. Notably, the positive node of the circuit should be always grounded to provide continuous electrons, and the function of the TENG is to pump electrons to the carbon fibre electrodes. The working mechanisms are similar to the switch-controlled process and are presented in detail in Supplementary Fig. 7a,b. Because there is no short-circuit process for equilibrating the TENG device at Status I and III, the V–Q plots with a rectifying circuit (ideal condition) depicted in Supplementary Fig. 7c,d are different from those in Fig. 3a,b. Nevertheless, owing to the high open-circuit voltage, the FS-TENG operates close to the reported baseline and ion quantities are not significantly affected. For the CS-TENG, the diode during the contacting process naturally forms a short circuit of two electrodes,
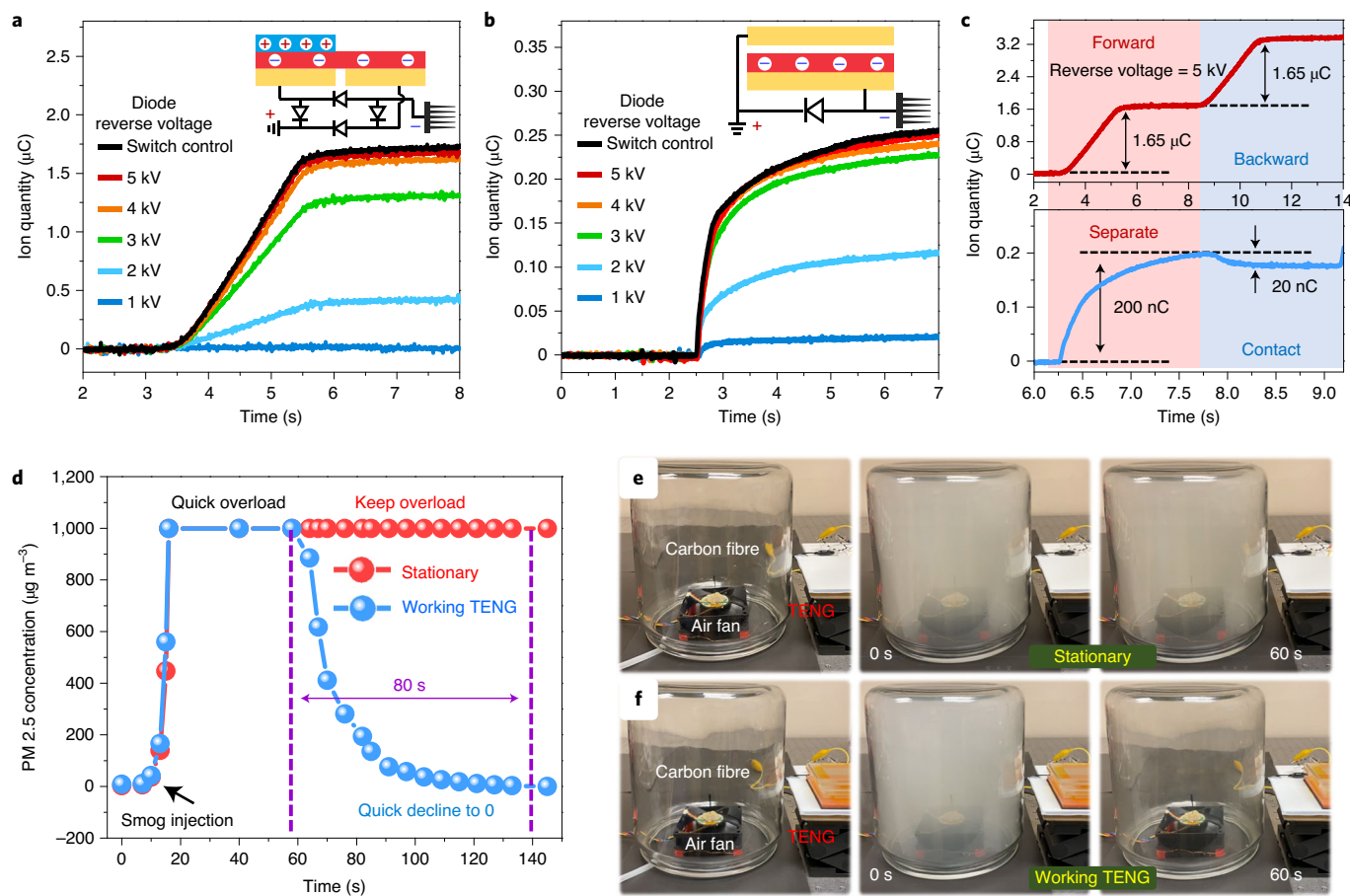
Fig. 4 | Performance of the MSNG. a,b, NAI charge quantity produced with various circuit element parameters using the FS-TENG (**a**) and CS-TENG (**b**) in a forward and separating step, respectively. The insets show the circuits and TENG schemes. **c**, Dynamic ion quantity curve of the FS- and CS-TENGs during a full operational period. **d**, Comparative measurements of the dynamic variation in PM 2.5 levels in a cylindrical chamber when operating and not operating the FS-TENG. **e,f**, Demonstration of the smog removing performance of the MSNG in stationary conditions (**e**) and with the FS-TENG operating at a frequency of 0.25 Hz (**f**).

and thus the NAI quantity is the same as the switch-controlled one. In practical conditions, the reverse voltage of each diode element in the rectifying circuit limits the maximal potential of the carbon electrodes, which may significantly impact the NAI productivity. As shown in Fig. 4a,b, the NAI quantity (that is, the NAI density presented in Supplementary Fig. 8) increases as the reverse voltage increases and saturates near the switch-controlled value when the reverse voltage reaches 5 kV. In Fig. 4c, for a full working period, the NAI generation properties of the MSNG with a 5 kV reverse voltage are also highly similar to those of the switch-controlled TENGs (the possible mechanisms of the reverse charge drop for the CS-TENG are depicted in Supplementary Fig. 9). Notably, the ion quantity is constant during multiple working cycles (Supplementary Fig. 10). With that in mind, although diode elements with lower reverse voltages could potentially reduce NAI quantity, they also suppress the production of harmful NAIs (for example, ozone⁻ and oxynitride⁻) for some specific applications. Finally, to further prove its functionality, we explored the potential of the MSNG as an air particulate matter removal technology. As depicted in Supplementary Fig. 11, a carbon fibre electrode fixed on an air fan (used for circulating air) was placed in an enclosed glass chamber with a volume of 5,086 cm³, and PM 2.5 was generated by a burning cigarette, monitored by an air pollution meter. As shown in Fig. 4d, upon smog injection, the PM 2.5 level rises dramatically to an overload level (999 µg m⁻³), remaining constant for the period of the test under stationary

conditions. In contrast, the PM 2.5 rapidly declines to 0 µg m⁻³ in 80 s while operating the FS-TENG at a frequency of 0.25 Hz. The dynamic air purification process and mechanism are illustrated in Fig. 4d and Supplementary Video 1, and are schematically depicted in Supplementary Fig. 12. Moreover, the observable heavy smog removal process is exhibited in Fig. 4e,f and Supplementary Video 2, which illustrate the efficient air purification ability of the MSNG and its potential application in greatly increasing the sustainability of industries while protecting the environment.

Conclusions
In summary, we have demonstrated a corona-type MSNG using the high output voltage of a TENG and carbon fibre electrodes. NAIs produced by the MSNG were quantified and identified using an air ion counter and mass spectrometer. A unique testing platform was designed for quantitatively recording the NAI quantity and analysing the ionization process. The basic FS- and CS-TENGs, which are capable of converting the vast majority of otherwise wasted mechanical energy sources, readily achieved the threshold voltage of air ionization with carbon fibre electrodes, and the electron–ion transformation efficiencies of these TENGs reached 97 and 70%, respectively. The designed switch-controlled process for maximally using the output of the TENGs and the circuit-controlled process for on-demand NAI generation were both studied in detail using V–Q plots. To demonstrate the MSNG's ability to remove PM 2.5, a palm-sized device

produced 1×10^{13} NAIs in one sliding motion and purified the PM 2.5 from 999 to 0 µg m^{-3} in a 5,086 cm^3 glass chamber within 80 s under an operational frequency of 0.25 Hz using the FS-TENG. The advantages of NAI-generating TENGs, including their portability, low-frequency motion-harvesting efficiency, material variety and low cost, clearly present them as an economic, facile and safe approach to progressing our drive for a more sustainable society.

Methods

Fabrication of the MSNG. The fabrication process of the MSNG can be divided into the preparation of the TENG component, rectifying circuit module and air ionization electrode. In this work, an FS- and CS-TENG were both used in our experiments. For the FS-TENG, copper foil was first attached to a 125 mm × 70 mm acrylic sheet. The copper foil was then covered by a 50-µm-thick PTFE film after creating an gap of 5 mm to act as a stator. Next, a 60 × 70 mm polyurethane foam layer was attached to an acrylic sheet of the same size as the slider. For the CS-TENG, the top layer was constructed by attaching copper foil to an acrylic board (70 mm × 70 mm) and the bottom layer (70 mm × 70 mm) was fabricated by physical vapour deposition of 0.1 µm copper on a 50-µm-thick PTFE film, also supported on an acrylic sheet. The rectifier module was composed of four diodes for the FS-TENG-based MSNG and one diode for the CS-TENG MSNG. In particular, the four diodes constructed a full-wave rectifier, and each diode also consisted of several diodes in series connection to increase the reverse voltage. A carbon fibre with a single wire diameter of 10 µm (Alibaba) was cut into several bunches with lengths of 2 cm and fixed on a uniformly perforated acrylic sheet as the air ionization electrodes (Supplementary Fig. 2). Finally, each part was electrically connected. Specifically, the negative pole of the rectifier module was connected to the carbon fibre and the positive side was grounded.

Electric measurement and characterization. A field-emission scanning electron microscope (Hitachi SU8010) was used to characterize the morphologies of the carbon fibre electrodes and the nanostructured PTFE film. The NAIs were quantified and analysed by an air ion counter (Model AIC2, AlphaLab) and Q-Exactive hybrid quadrupole Orbitrap mass spectrometer (Thermo Scientific). The NAI charge testing platform is shown in Supplementary Fig. 4 and the ion charge quantity, open-circuit voltage and short-circuit transferred charge were recorded using a programmable electrometer (Keithley 6514). An air quality monitor (Amazon) was used for PM 2.5 testing. The software platform was constructed on the basis of LabVIEW, which is capable of realizing real-time data acquisition control and analysis.

Data availability

The data that support the plots within this paper and other findings of this study are available from the corresponding authors (V.K.S.H. and Z.L.W.) upon reasonable request.

References

1. Krueger, A. P. & Reed, E. J. Biological impact of small air ions. *Science* **193**, 1209–1213 (1976).
2. Jiang, S. Y., Ma, A. & Ramachandran, S. Negative air ions and their effects on human health and air quality improvement. *Int. J. Mol. Sci.* **19**, 2966 (2018).
3. Ryushi, T. et al. The effect of exposure to negative air ions on the recovery of physiological responses after moderate endurance exercise. *Int. J. Biometeorol.* **41**, 132–136 (1998).
4. Sawant, V. S., Meena, G. S. & Jadhav, D. B. Effect of negative air ions on fog and smoke. *Aerosol Air Qual. Res.* **12**, 1007–1015 (2012).
5. Livanova, L. M., Levshina, I. P., Nozdracheva, L. V., Elbakidze, M. G. & Airapetyants, M. G. The protective effects of negative air ions in acute stress in rats with different typological behavioral characteristics. *Neurosci. Behav. Physiol.* **29**, 393–395 (1999).
6. Wu, C. C. & Lee, G. W. M. Oxidation of volatile organic compounds by negative air ions. *Atmos. Environ.* **38**, 6287–6295 (2004).
7. Lin, H. F. & Lin, J. M. Generation and determination of negative air ions. *J. Anal. Test.* **1**, 6 (2017).
8. Richardson, G., Eick, S. A., Harwood, D. J., Rosen, K. G. & Dobbs, F. Negative air ionisation and the production of hydrogen peroxide. *Atmos. Environ.* **37**, 3701–3706 (2003).
9. Peterson, M. S., Zhang, W., Fisher, T. S. & Garimella, S. V. Low-voltage ionization of air with carbon-based materials. *Plasma Sources Sci. Technol.* **14**, 654–660 (2005).
10. Chen, C. H., Huang, B. R., Lin, T. S., Chen, I. C. & Hsu, C. L. A new negative ion generator using ZnO nanowire array. *J. Electrochem. Soc.* **153**, G894–G896 (2006).
11. Nakamura, T. & Kubo, T. Tourmaline group crystals reaction with water. *Ferroelectrics* **137**, 13–31 (1992).
12. Yeh, J. T. et al. Negative air ion releasing properties of tourmaline/bamboo charcoal compounds containing ethylene propylene diene terpolymer/polypropylene composites. *J. Appl. Polym. Sci.* **113**, 1097–1110 (2009).
13. Fan, F. R., Tian, Z. Q. & Wang, Z. L. Flexible triboelectric generator! *Nano Energy* **1**, 328–334 (2012).
14. Wu, C. S., Wang, A. C., Ding, W. B., Guo, H. Y. & Wang, Z. L. Triboelectric nanogenerator: a foundation of the energy for the new era. *Adv. Energy Mater.* **9**, 1802906 (2019).
15. Guo, H. Y. et al. A highly sensitive, self-powered triboelectric auditory sensor for social robotics and hearing aids. *Sci. Robot.* **3**, eaat2516 (2018).
16. Liu, W. L. et al. Integrated charge excitation triboelectric nanogenerator. *Nat. Commun.* **10**, 1426 (2019).
17. Liu, Y. et al. Quantifying contact status and the air-breakdown model of charge-excitation triboelectric nanogenerators to maximize charge density. *Nat. Commun.* **11**, 1599 (2020).
18. Hinchet, R. et al. Transcutaneous ultrasound energy harvesting using capacitive triboelectric technology. *Science* **365**, 491–494 (2019).
19. Xu, W. H. et al. A droplet-based electricity generator with high instantaneous power density. *Nature* **578**, 392–396 (2020).
20. Chen, L. et al. Controlling surface charge generated by contact electrification: strategies and applications. *Adv. Mater.* **30**, 1802405 (2018).
21. Shi, Q., He, T. & Lee, C. More than energy harvesting – combining triboelectric nanogenerator and flexible electronics technology for enabling novel micro-/nano-systems. *Nano Energy* **57**, 851–871 (2019).
22. Liu, S., Wang, H., He, T., Dong, S. & Lee, C. Switchable textile-triboelectric nanogenerators (S-TENGs) for continuous profile sensing application without environmental interferences. *Nano Energy* **69**, 104462 (2020).
23. Leung, S. et al. A self-powered and flexible organometallic halide perovskite photodetector with very high detectivity. *Adv. Mater.* **30**, 1704611 (2018).
24. Zi, Y. L. et al. Harvesting low-frequency (<5 Hz) irregular mechanical energy: a possible killer application of triboelectric nanogenerator. *ACS Nano* **10**, 4797–4805 (2016).
25. Li, A. Y., Zi, Y. L., Guo, H. Y., Wang, Z. L. & Fernandez, F. M. Triboelectric nanogenerators for sensitive nano-coulomb molecular mass spectrometry. *Nat. Nanotechnol.* **12**, 481–487 (2017).
26. Li, C. J. et al. Self-powered electrospinning system driven by a triboelectric nanogenerator. *ACS Nano* **11**, 10439–10445 (2017).
27. Zi, Y. L. et al. Field emission of electrons powered by a triboelectric nanogenerator. *Adv. Funct. Mater.* **28**, 1800610 (2018).
28. Cheng, J. et al. Triboelectric microplasma powered by mechanical stimuli. *Nat. Commun.* **9**, 3733 (2018).
29. Kim, H. J., Han, B., Woo, C. G. & Kim, Y. J. Ozone emission and electrical characteristics of ionizers with different electrode materials, numbers, and diameters. *IEEE Trans. Ind. Appl.* **53**, 459–465 (2017).
30. Kim, H. J., Han, B., Kim, Y. J., Oda, T. & Won, H. Submicrometer particle removal indoors by a novel electrostatic precipitator with high clean air delivery rate, low ozone emissions, and carbon fiber ionizer. *Indoor Air* **23**, 369–378 (2013).
31. Tyndall, A. M., Starr, L. H. & Powell, C. F. The mobility of ions in air. Part IV.—Investigations by two new methods. *Proc. R. Soc. Lond. A* **121**, 172–184 (1928).
32. Skalny, J. D. et al. Mass spectrometric study of negative ions extracted from point to plane negative corona discharge in ambient air at atmospheric pressure. *Int. J. Mass Spectrom.* **272**, 12–21 (2008).
33. Wu, C. C., Lee, G. W. M., Yang, S., Yu, K. P. & Lou, C. L. Influence of air humidity and the distance from the source on negative air ion concentration in indoor air. *Sci. Total Environ.* **370**, 245–253 (2006).
34. Lin, L., Li, Y., Khan, M., Sun, J. S. & Lin, J. M. Real-time characterization of negative air ion-induced decomposition of indoor organic contaminants by mass spectrometry. *Chem. Commun.* **54**, 10687–10690 (2018).
35. Sabo, M., Okuyama, Y., Kucera, M. & Matejcik, S. Transport and stability of negative ions generated by negative corona discharge in air studied using ion mobility-oaTOF spectrometry. *Int. J. Mass Spectrom.* **334**, 19–26 (2013).
36. *COMSOL Multiphysics* v.5.2a (COMSOL, 2016); https://cn.comsol.com/comsol-multiphysics
37. Zi, Y. L. et al. Standards and figure-of-merits for quantifying the performance of triboelectric nanogenerators. *Nat. Commun.* **6**, 8376 (2015).

Author contributions

Competing interests

The authors declare no competing interests.

Additional information

Supplementary information is available for this paper at https://doi.org/10.1038/s41893-020-00628-9.

Correspondence and requests for materials should be addressed to V.K.S.H. or Z.L.W.

Reprints and permissions information is available at www.nature.com/reprints.

Publisher's note Springer Nature remains neutral with regard to jurisdictional claims in published maps and institutional affiliations.